

Hidden excitonic quantum states with broken time-reversal symmetry

Giacomo Mazza^{1,2,*} and Marco Polini^{1,3,4}

¹*Dipartimento di Fisica dell'Università di Pisa, Largo Bruno Pontecorvo 3, I-56127 Pisa, Italy*

²*Department of Quantum Matter Physics, University of Geneva, Quai Ernest-Ansermet 24, 1211 Geneva, Switzerland*

³*Istituto Italiano di Tecnologia, Graphene Labs, Via Morego 30, I-16163 Genova, Italy*

⁴*ICFO-Institut de Ciències Fotòniques, The Barcelona Institute of Science and Technology, Av. Carl Friedrich Gauss 3, 08860 Castelldefels (Barcelona), Spain*

The spontaneous breaking of time-reversal symmetry due to purely-orbital mechanisms (i.e. not involving spin degrees of freedom) yields extremely exotic phases of matter such as Chern insulators and chiral superconductors. In this Letter, we show that excitonic insulators, by exploiting the transition from the excitonic ground state to a purely-orbital time reversal symmetry broken hidden state, can realize another notable example of this class. The transition to the hidden state is controlled by engineered geometrical constraints which enable the coupling between the excitonic order parameter and the free-space electromagnetic field. These results pave the way towards exotic orbital magnetic order in quantum materials and are also relevant for disentangling excitonic phase transitions from trivial structural ones.

I. INTRODUCTION

The physical properties of a condensed matter system are often direct manifestations of well defined processes of spontaneous symmetry breaking. Examples range from the breaking of translation symmetry in the formation of crystalline solids, to the breaking of time-reversal symmetry in magnetic systems and particle conservation in superconductors [1]. In some cases, however, the nature of symmetry breaking alone may not be enough to fully determine the physical properties of the system. This can happen in the case of excitonic phase transitions [2] in which electronic states belonging to valence and conduction bands spontaneously hybridize due to the Coulomb interaction between negatively charged electrons and positively charged holes.

The phenomenon of exciton condensation is well studied in heterostructures with spatially separated electrons and holes [3–8]. Nonetheless, the formation of a so-called excitonic insulator state in crystalline solids remains a debated question [9–14]. The main reason is that the excitonic instability can generically lead to different physical manifestations depending on the degrees of freedom it couples with. For example, the excitonic instability may induce a distortion of the charge density which, due to the coupling with the ionic degrees of freedom, makes the excitonic state practically indistinguishable from a structural phase transition [15–21].

In this Letter, we exploit a dichotomic manifestation of the symmetry breaking underlying an excitonic phase transition to show the stabilization of a time-reversal symmetry broken (TRSB) hidden quantum state in a two-dimensional (2D) material by means of engineered geometrical constraints. Fig. 1 summarizes the main result of this Letter: The ground state of a 2D material

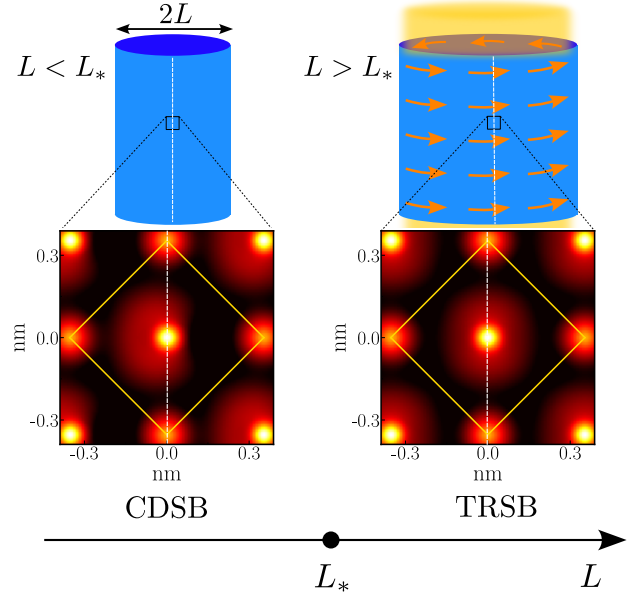


Figure 1. Schematic phase diagram of the excitonic ground state as a function of the cylinder radius L . The color plots show the charge density distributions in the unit cells (indicated by yellow squares) for $L < L_*$ and $L > L_*$. The white dashed lines highlight the reflection symmetry broken by the excitonic instability. In the CDSB state the charge density is not invariant under the reflection symmetry. The TRSB state displays a solenoidal persistent current being characterised by a symmetric charge density. The yellow shading is a pictorial representation of the self-generated flux that sustains the persistent current.

harboring an excitonic phase transition, in a cylinder geometry, can be transformed from a charge-density symmetry broken (CDSB) state to a TRSB one (which hosts persistent orbital currents) by controlling the cylinder radius.

The change in the ground state nature is driven by a self-generated flux which sustains the equilibrium orbital

* giacomo.mazza@unipi.it

currents, and lowers the energy of the hidden excitonic TRSB state with respect to the energy of the CDSB ground state. We predict the transition to occur for cylinders with radius larger than a critical value, which can be further controlled by an applied external flux.

II. MODEL AND PURELY ELECTRONIC INSTABILITY.

We consider a system of interacting electrons subject to a 2D potential with the periodicity of a square lattice, $V(\mathbf{x}) = V(\mathbf{x} + \mathbf{R})$. The crystalline potential $V(\mathbf{x}) = \sum_{\mathbf{R},a} v_a(\mathbf{x} - \mathbf{R})$ originates from atomic-like potential wells $v_a(\mathbf{x} - \mathbf{R})$ centered at the position of an atom of type a in the unit cell \mathbf{R} . Specifically, we consider two atoms $a = A, A'$ per unit cell, arranged as in Fig. 2(a). We choose atomic potentials of the Yukawa type, i.e. $v_a(\mathbf{x}) = -\gamma_a e^{-|\mathbf{x}|/\xi_a} / (|\mathbf{x}| + \eta_a)$, where η_a is a short-distance cut-off. We solve Bloch eigenvalue problem and adjust the parameters γ_a, ξ_a , and η_a in order to obtain a band structure in which bands originating from atomic-like orbitals of different symmetry overlap at the Fermi level. In this work we consider spinless fermions and an excitonic instability that occurs only in the spin singlet channel [27].

By assuming four electrons per unit cell, they have a bandwidth $W \sim 4$ eV and mainly originate from the $2s$ orbital and $1p_{\pm} = 1p_x \pm i1p_y$ orbitals of the central atom (Fig. 2(b)). The three low-energy bands are occupied by two electrons, whereas two additional electrons occupy two core bands (not shown) originating, respectively, from the $1s$ orbitals of the central and corner atoms. We derive localized Wannier wavefunctions using the projection method [28] and write the single-particle band Hamiltonian in the Wannier basis as $\mathcal{H}_0 = \sum_{\mathbf{R},\mathbf{R}'} \sum_{\alpha,\beta=s,p_{\pm}} h_{\mathbf{R},\mathbf{R}'}^{\alpha\beta} c_{\mathbf{R},\alpha}^{\dagger} c_{\mathbf{R}',\beta}$. The Wannier wavefunctions are mainly localized on the central atom, with weaker amplitude on the corner atoms—see Fig. 2(c). The s -like wave-function is even under reflection with respect to the two axes $y = \pm x$, whereas the p_{\pm} -like ones are odd/even under reflections with respect to the $y = \pm x/\mp x$ axes, respectively.

Due to the above symmetries, the local matrix elements of the single-particle Hamiltonian \mathcal{H}_0 between s - and p -like orbitals identically vanish, i.e. $h_{\mathbf{R},\mathbf{R}}^{sp_{\pm}} = 0$, implying a vanishing local hybridization between s and p_{\pm} Wannier wave-functions:

$$\Delta_{\pm}^{(0)} \equiv \langle c_{\mathbf{R},s}^{\dagger} c_{\mathbf{R},p_{\pm}} \rangle = 0. \quad (1)$$

The hybridizations in Eq. (1) play the role of order parameters for the breaking of the symmetries of the square lattice due to the excitonic instability. With this target in mind, we add to the bare band Hamiltonian \mathcal{H}_0 two electron-electron interaction contributions: i) a purely local density-density interaction U between p_+ and p_-

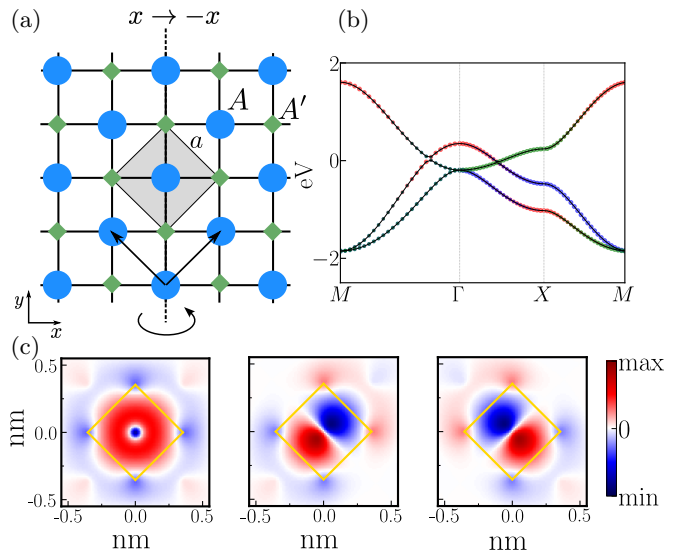


Figure 2. (a) 2D crystal structure. Big (blue) circles and small (green) diamonds represent the positions of the two atomic-like potential wells, A and A' , respectively. The shaded area denotes the unit cell, while $a = 0.5$ nm indicates the lattice parameter. The dashed line represents the reflection symmetry broken by the excitonic instability in the channel $\Delta_+ = -i\Delta_- = \Delta$. The arrows indicate the primitive vectors of the Bravais lattice. The curved arrow indicates the wrapping around the y -axis discussed in this work. (b) Fat band representation of the low-energy band structure. The band structure is obtained by setting (see main text): $\gamma_A = 1.52$ eV nm, $\gamma_{A'} = 0.38$ eV nm, $\xi_A = \xi_{A'} = 1$ nm, and $\eta_A = \eta_{A'} = 10^{-3}$ nm. Red, green, and blue projections correspond, respectively, to the s , p_+ , and p_- Wannier orbitals. (c) Real-space maps of the s , p_+ , and p_- Wannier orbitals (from left to right).

Wannier orbitals, and ii) a density-density interaction V between s and p_{\pm} orbitals. The full Hamiltonian therefore reads:

$$\mathcal{H} = \mathcal{H}_0 + U \sum_{\mathbf{R}} n_{\mathbf{R},p_+} n_{\mathbf{R},p_-} + V \sum_{\mathbf{R},\alpha=\pm} n_{\mathbf{R},p_{\alpha}} n_{\mathbf{R},s}. \quad (2)$$

For the sake of concreteness, we fix $U = 2.5$ eV and $V = 2.0$ eV, of the same order of magnitude of the bandwidth W .

Seeking for the excitonic instability, we introduce a family of variational wave-functions $|\Psi_{\Delta}\rangle$, corresponding to BCS wave functions with pairing in the particle-hole channel, and allow for a non-vanishing order parameter

$$\Delta_{\pm} \equiv \langle \Psi_{\Delta} | c_{\mathbf{R},p_{\alpha}}^{\dagger} c_{\mathbf{R},s} | \Psi_{\Delta} \rangle \neq 0. \quad (3)$$

By introducing Lagrange multipliers λ_{\pm} , we compute the variational energy as a function of Δ_{\pm} :

$$E_{\text{var}}[\Delta_{\pm}, \lambda_{\pm}] = \langle \Psi_{\Delta} | \mathcal{H} | \Psi_{\Delta} \rangle + \sum_{\mathbf{R},\alpha=\pm} \lambda_{\alpha} \left(\langle \Psi_{\Delta} | c_{\mathbf{R},p_{\alpha}}^{\dagger} c_{\mathbf{R},s} | \Psi_{\Delta} \rangle - \Delta_{\alpha} \right) + \text{c.c.} \quad (4)$$

For a given Δ_{\pm} , we self-consistently optimize the variational wave-function with respect to the Lagrange multipliers and all the expectation values $\Delta_{\mathbf{k}}^{\alpha,\beta} = \langle \Psi_{\Delta} | c_{\mathbf{k},\alpha}^{\dagger} c_{\mathbf{k},\beta} | \Psi_{\Delta} \rangle$. We restrict our analysis to the channel $\Delta_{+} = -i\Delta_{-}$, which we found as the most stable channel for symmetry breaking in the model. Such combination of order parameters corresponds to the breaking of reflection symmetry $x \rightarrow -x$ (see Fig. 2). As a result, the energy functional in Eq. (4) reduces to a function of a single order parameter $\Delta = |\Delta|e^{i\varphi} \equiv \Delta_{+}$. We notice that, as a consequence of the $s - p_{\pm}$ hybridizations, the symmetry broken state automatically displays a non-zero $p_{+} - p_{-}$ hybridization $\Delta_{pp} \equiv \langle \Psi_{\Delta} | c_{p_{+}}^{\dagger} c_{p_{-}} | \Psi_{\Delta} \rangle \neq 0$ due to broken 4-fold rotation symmetry of the square lattice.

The nature of the excitonic states issuing from the breaking of the $x \rightarrow -x$ symmetry depends on the order parameter phase φ [25, 26]. This is readily understood from simple arguments of quantum mechanics. Let us consider two generic real wavefunctions $\Psi_e(x, y) = \Psi_e(-x, y)$ and $\Psi_o(x, y) = -\Psi_o(-x, y)$, which are even and odd, respectively, under the $x \rightarrow -x$ reflection symmetry. The excitonic order parameter corresponds to an hybridized state $\Psi(\mathbf{x}) \sim \Psi_e(\mathbf{x}) + |\Delta|e^{i\varphi}\Psi_o(\mathbf{x})$. By computing the charge $\rho(\mathbf{x}) \equiv \Psi^{*}(\mathbf{x})\Psi(\mathbf{x})$ and momentum $\mathbf{p}(\mathbf{x}) \equiv -\frac{i}{2}\hbar\Psi^{*}(\mathbf{x})\nabla\Psi(\mathbf{x}) + c.c.$ densities, it is straightforward to see that for $\varphi = 0, \pi$ $\Psi(\mathbf{x})$ corresponds to a CDSB state with $\rho(x, y) \neq \rho(-x, y)$, and which displays time-reversal symmetry, $\mathbf{p}(\mathbf{x}) = 0$. On the contrary, for $\varphi = \pm\frac{\pi}{2}$, it corresponds to a TRSB state with $\mathbf{p}(-x, y) \neq -\mathbf{p}(x, y)$, and a symmetric charge density $\rho(\mathbf{x}) = \rho(-\mathbf{x})$. For a generic $\varphi \neq 0, \pi, \pm\frac{\pi}{2}$, $\Psi(\mathbf{x})$ describes at the same time a CDSB and TRSB state.

We explicitly show the CDSB and TRSB characters of the variational states $|\Psi_{\Delta}\rangle$ by computing the quantities $\delta\rho \equiv \int_{x<0} \rho_{\Delta}(\mathbf{x})d^2\mathbf{x} - \int_{x>0} \rho_{\Delta}(\mathbf{x})d^2\mathbf{x}$ and $\mathbf{P} \equiv \int_{x<0} \mathbf{p}_{\Delta}(\mathbf{x})d^2\mathbf{x} + \int_{x>0} \mathbf{p}_{\Delta}(\mathbf{x})d^2\mathbf{x}$ for fixed order parameter modulus $|\Delta|$ and varying phase φ . “ $\int_{x</>0}$ ” means integration over the two portions of the unit cells separated by the $x = 0$ axis, and $\rho_{\Delta}(\mathbf{x})$ and $\mathbf{p}_{\Delta}(\mathbf{x})$ are density and momentum densities computed on the variational state $|\Psi_{\Delta}\rangle$ by expanding the fermionic fields over the complete set of Bloch wave-functions $\Psi(\mathbf{x}) = \sum_{\mathbf{k},n} \psi_{\mathbf{k},n}(\mathbf{x})c_{\mathbf{k},n}$. For $\varphi = 0$, we find $\delta\rho \neq 0$, and $P_x = P_y = 0$ highlighting the pure CDSB nature of the excitonic state—see Fig. 3(a). Increasing φ , the CDSB contribution $\delta\rho$ decreases and the excitonic states acquire TRSB character, as highlighted by $\mathbf{P} \neq 0$. Eventually, the CDSB vanishes for $\varphi = \pi/2$, where the TRSB contribution \mathbf{P} is maximum. We notice that the TRSB excitonic state corresponds to a net momentum through the unit cell along the x direction. On the contrary, the reflection symmetry $y \rightarrow -y$ is preserved and the net momentum along the y direction is identically zero.

In Fig. 3(b) we plot the variational energy as a function of the real and imaginary parts of the order parameter Δ . The energy surface displays two equivalent global minima

at $|\Delta| \neq 0$ which highlight the spontaneous symmetry breaking and reflect the Z_2 nature of the broken reflection symmetry $x \rightarrow -x$. The two minima corresponds to real order parameters $\varphi = 0, \pi$, thus showing that, for the purely electronic instability, the excitonic ground state corresponds to the CDSB state.

III. TRSB EXCITONIC STATE.

All the TRSB states obtained by the variational optimization of Eq. (4) are unstable hidden states with energy higher than the CDSB states at $\varphi = 0, \pi$. This result is in agreement with the no-go theorems that forbid a ground state with a non-vanishing *net* current. The argument, originally attributed to Bloch [29], follows from the observation that the energy of a state with net current can be made arbitrary small by an unphysical constant vector potential (i.e. unphysical since it can be gauged away).

We now show that, indeed, the TRSB excitonic state can be stabilized by: i) changing the topology of the system and ii) allowing the TRSB state to act as a source of a physical magnetic flux. We start by wrapping the 2D system on a cylinder of radius L around the y -axis—see Fig. 2(a). In this cylindrical geometry, the current of the TRSB state is purely solenoidal. The net current vanishes and the state couples only to physical fields that cannot be gauged away. Moreover, in this geometry the TRSB state can source a magnetic flux which is naturally expected to lead to an energy lowering. Indeed, the fact that, in nature, currents act as sources of a magnetic flux simply implies that the energy of the TRSB state including the flux sourced by the TRSB state itself should have energy lower than the energy of the TRSB state without self-generated flux. In the following, we show that, in this geometry, such an energy lowering is controlled by the cylinder radius.

We introduce a new energy functional $\mathcal{E}[\Delta, \mathbf{A}, \lambda]$ which depends on the excitonic order parameter Δ , the associated Lagrange parameter λ , and on a self-generated, purely transverse ($\nabla \cdot \mathbf{A} = 0$), vector potential \mathbf{A}

$$\begin{aligned} \mathcal{E}[\Delta, \mathbf{A}, \lambda] = & E_{\text{var}}[\Delta, \lambda] + \int_{\mathbf{v}} d^3\mathbf{r} \frac{[\nabla \times \mathbf{A}(\mathbf{r})]^2}{2\mu_0} + \\ & + \frac{e}{m} \int_{\mathbf{s}} d^2\mathbf{x} \mathbf{p}_{\Delta}(\mathbf{x}) \cdot \mathbf{A}(\mathbf{x}) + \\ & + \frac{e^2}{2m} \int_{\mathbf{s}} d^2\mathbf{x} \rho_{\Delta}(\mathbf{x}) \mathbf{A}^2(\mathbf{x}), \end{aligned} \quad (5)$$

where m is the bare electron mass in vacuum, μ_0 is the vacuum magnetic permeability, and $\int_{\mathbf{v}} d^3\mathbf{r}$ ($\int_{\mathbf{s}} d^2\mathbf{x}$) indicates the volume (surface) integral over the full space (restricted to cylinder). $E_{\text{var}}[\Delta, \lambda]$ represents the variational electronic energy for the cylindrical geometry. We assume $L \gg a$, so that we can neglect the local curvature of the cylinder and treat, for all the practical purposes,

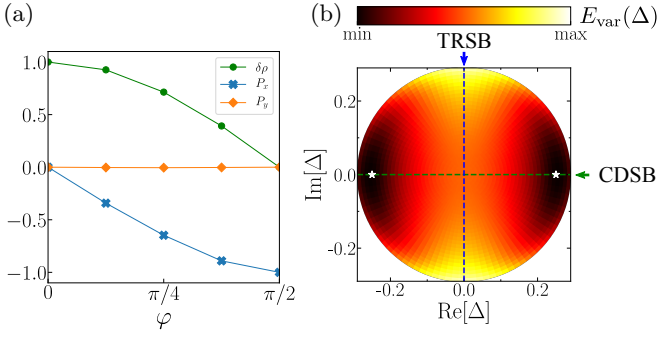


Figure 3. (a) Quantifiers $\delta\rho$ and \mathbf{P} (see main text) of the CDSB and TRSB character of a generic state $|\Psi_\Delta\rangle$ at a fixed value of $|\Delta| = 0.25$ and varying phase φ . $\delta\rho$ is measured with respect to its $\varphi = 0$ value, whereas $P_{x/y}$ components are measured with respect to their $\varphi = \pi/2$ values. (b) Variational energy for the pure electronic problem as a function of $\text{Re}(\Delta)$ and $\text{Im}(\Delta)$. The white stars indicate the two global minima while the dashed horizontal (vertical) line highlights the purely CDSB (TRSB) state.

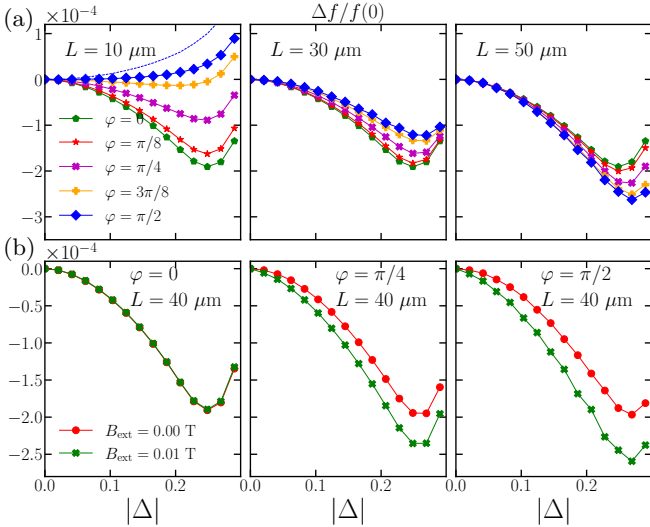


Figure 4. (a) Volume energy density $f(\Delta)$ as a function of $|\Delta|$, for different values of φ —from the pure CDSB (green pentagons) state at $\varphi = 0$ to the pure TRSB (blue diamonds) state at $\varphi = \pi/2$ —and different values of the cylinder radius L . All the energies are measured with respect to the energy $f(0)$ in the $\Delta = 0$ symmetric case— $\Delta f \equiv f(\Delta) - f(0)$ —and in units of $f(0)$. In the $L = 10 \mu\text{m}$ panel the dashed line represents the energy density for the $\pi/2$ state for the purely electronic problem in the absence of self-generated flux. (b) Volume energy density of the pure CDSB state (left) and the pure TRSB state (right) as a function of an applied external flux and $L = 40 \mu\text{m}$.

the electronic system as a 2D system with physical periodic boundary conditions.

Imposing that \mathcal{E} is stationary with respect to the vector potential, i.e. $\delta\mathcal{E}/\delta\mathbf{A} = 0$, yields Ampere's law:

$$-\nabla^2 \mathbf{A} = \mu_0 \mathbf{J}[\mathbf{A}, \Delta], \quad (6)$$

where, in cylindrical coordinates $\mathbf{r} = (r, \theta, y)$, the volume current density reads

$$\mathbf{J}[\mathbf{A}, \Delta] = -\frac{e}{m} \delta(r-L) [\mathbf{p}_\Delta(\mathbf{x}) + e\rho_\Delta(\mathbf{x})\mathbf{A}(\mathbf{r})]. \quad (7)$$

$\mathbf{x} = (L \sin \theta, L \cos \theta, y)$ represents a point on the cylinder surface, and $\rho_\Delta(\mathbf{x})$ and $\mathbf{p}_\Delta(\mathbf{x})$ are the charge and momentum surface density computed for the excitonic state $|\Psi_\Delta\rangle$ and in the presence of the vector potential \mathbf{A} .

Solving Eq. (6) allows to eliminate \mathbf{A} and express the energy \mathcal{E} as a function of Δ only. To this extent, we coarse grain the charge and momentum density by averaging over the unit cell. In doing so, we obtain a TRSB state with a uniform charge density ρ_0 and a uniform solenoidal momentum density $\mathbf{p}_\Delta = \theta \mathbf{P}_\Delta$. This approximation corresponds to neglecting contributions of the flux which are i) perpendicular to the cylinder surface and ii) vary over length scales smaller than the lattice parameter.

Ampere's equation is solved by a solenoidal vector potential $\mathbf{A}(\mathbf{r}) = \theta A_\Delta [(L/r)\theta_H(r-L) + (r/L)\theta_H(L-r)]$. Here, θ_H is the Heaviside step function, and we have fixed the gauge by requiring the vector potential to vanish for $r/L \rightarrow \infty$. The solenoidal vector potential A_Δ depends on the average momentum of the TRSB state and on the radius L as following:

$$A_\Delta = -\Phi_0 \frac{P_\Delta}{h\rho_0 \ell_0 + L}. \quad (8)$$

Here, $\Phi_0 = h/e$ is the flux quantum and $\ell_0 \equiv 2m/(\mu_0 e^2 \rho_0) \simeq 3.5 \mu\text{m}$ is a characteristic length scale of the problem set by the electronic density $\rho_0 = 4/a^2$. We emphasize that, in Eq. (8), P_Δ is the average momentum density computed for the variational state $|\Psi_\Delta\rangle$, and in the presence of the solenoidal vector potential A_Δ , so that, eventually, P_Δ and A_Δ are simultaneously determined by the solution of the variational problem.

For a given P_Δ , the self-generated vector potential leads to a partial cancellation of the paramagnetic current that characterizes the TRSB state. This fact results in a gain of the electronic kinetic energy which will be balanced by the positive magnetic energy due to the self-generated flux. In order to estimate these contributions, we notice that the electronic energy is proportional to the cylinder surface, whereas the magnetic energy is proportional to the cylinder volume. We therefore consider the total volume energy density by normalizing the total energy over the volume of the cylinder $f \equiv \mathcal{E}/(\pi L^2 L_z)$. Here, $\mathcal{E} = \mathcal{E}_e + \mathcal{E}_m$, with \mathcal{E}_e/m represent, respectively, the electronic/magnetic contributions and the limit of an infinitely-long cylinder $L_z \rightarrow \infty$ is understood. Denoting with $E_e^{2D} = \frac{\mathcal{E}_e}{2\pi L L_z}$ the electronic surface energy density, and with $E_m^{3D} = \frac{\mathcal{E}_m}{\pi L^2 L_z}$ the magnetic volume energy density, the total volume energy density reads

$$f = E_m^{3D} + \frac{2E_e^{2D}}{L}. \quad (9)$$

The contribution to the electronic surface energy density can be estimated from the diamagnetic contribution to

the kinetic energy $E_{\text{kin}}(A) \sim \langle (P + eA)^2 \rangle$, which yields a negative contribution $\Delta E_e^{2D} \sim E_{\text{kin}}(A) - E_{\text{kin}}(A=0) \sim 2eA_\Delta P_\Delta + e^2 A_\Delta^2 \rho_0 = -\frac{P_\Delta^2}{\rho_0} \frac{L^2 + 2L\ell_0}{(\ell_0 + L)^2}$ that increases with the average momentum density, *i.e.* moving towards the pure TRSB state at $\varphi = \pi/2$. At fixed P_Δ , ΔE_e^{2D} increases sub-linearly with L/ℓ_0 , saturating for $L \gg \ell_0$, so that the electronic gain in the volume energy density scales as $\Delta E_e^{2d}/L \sim -P_\Delta^2 \frac{\ell_0}{L}$. On the contrary, by computing the flux density $\vec{B} = 2A_\Delta/L$, it is easy to check that the magnetic energy per unit volume $E_m^{3D} = B^2/2\mu_0$ decreases, for $L \gg \ell_0$, as $\Delta E_m^{3D} \sim P_\Delta^2 (\ell_0/L)^2$. This indicates that, by increasing the cylinder radius, the energy loss of the TRSB decreases faster than the energy gain. As a result, we expect the overall energy gain of the TRSB due to the sourcing of the magnetic flux to be negligible for $L \ll \ell_0$ and to become sizeable in the opposite limit.

We confirm the above expectations by solving the full variational problem, namely by self-consistently solving Eq. (8), together with the optimization of the Lagrange parameter and the variational wave-function $|\Psi_\Delta\rangle$ [30]. In Fig. 4(a) we compare the total volume energy densities at fixed cylinder radii for several phases moving from the pure CDSB to the pure TRSB. The energy of the pure CDSB state does not depend on L . On the contrary, the TRSB states experience an energy lowering which increases as a function of L . As the radius of the solenoid increases, the energy minimum shifts from the CDSB state to the TRSB state for $L > L_*$, with a critical radius $L_* \approx 40 \mu\text{m}$. In the TRSB state, the solenoid is characterized by a macroscopic magnetic moment sustained by a ground-state persistent solenoidal current, which represents an alternative manifestation of the spontaneous breaking of the $x \rightarrow -x$ crystal symmetry. In Fig. 4(b) we show that an external flux can further lower the energy barrier between the CDSB and TRSB states, thus highlighting the possibility of tuning the critical radius L_* .

We now comment on the limit of a large solenoid. In the limit $L/\ell_0 \rightarrow \infty$, the diamagnetic current perfectly cancels the paramagnetic one leading to a TRSB state with vanishing surface current density. We emphasize that, for any macroscopic value of L/ℓ_0 , the cylinder remains topologically distinct from an infinite 2D sheet. Such a distinction between the two geometries can be traced back to the fact that the TRSB is stabilized by self-generated magnetic flux which carries information about the geometry. Indeed, the solution of Ampere's equation in the cylindrical geometry enforces the physical vector potential to vanish for $r/L \rightarrow \infty$, whereas, for an infinite 2D sheet, the vector potential diverges for $r/L \rightarrow \infty$ [30]. In particular, at variance with the cylinder case, for an infinite 2D sheet the magnetic energy associated with the sourced flux would be infinite. As a result, no energy gain for the TRSB would be possible and the CDSB state remains the only stable state, in accordance to the aforementioned no-go theorems.

IV. DISCUSSION AND CONCLUSIONS.

We have shown a controlled path to the stabilization of a spontaneous TRSB phase of purely orbital character issuing from an excitonic instability. The TRSB state is achieved by topological constraints on the system which impose physical boundary conditions and enable the direct coupling between the excitonic order parameter and a self-generated magnetostatic potential that cannot be gauged away. The TRSB excitonic phase with self-generated vector potential is equivalent to the super-radiant excitonic insulating phase discussed in Ref. [35] once the no-go theorems about spatially-uniform vector potentials are properly taken into account [36–40].

Our results have direct implications on the disentangling of coupled excitonic and structural transitions. At variance with the CDSB state, the TRSB excitonic state is charge symmetric and is expected to have no direct coupling with lattice distortions. Estimating the relative energy gain between the lattice distortion and the flux generation discussed here is beyond the scope of this work. Nonetheless, the control of the energy barrier between the TRSB and CDSB states with an external flux—see Fig. 4—highlights the intriguing possibility of a magnetic tuning of coupled structural and excitonic phase transition. As such, our results suggest an equilibrium route for the disentangling of excitonic and structural phase transitions. For example, materials of interest include the above mentioned Ta_2NiSe_5 for which attempts to disentangle the two transitions focused so far only on the use of time-dependent probes [22–24]. We emphasize that the specific geometry for the stabilization of the TRSB phase depends on the precise symmetry of the order parameter and may vary from case to case. Specific material realizations and the interplay with lattice distortions represent natural directions for future research. This may include, for example, the interplay between geometrical constraints discussed here and the structured electromagnetic vacuum inside chiral cavities [41]. Moreover, our results can also have implications for other types of intertwined charge and chiral orders as discussed, for example, in the case of kagome metals [42, 43].

The experimental discovery of excitonic TRSB phases would provide us with an entirely new family of quantum systems displaying non-trivial time-reversal symmetry breaking of orbital origin, together with e.g. Chern insulators (such as those recently discovered in twisted bilayer graphene [44–48] and ABC-trilayer graphene [49]) and chiral superconductors (see, for example, Refs. 50–54 and references therein).

ACKNOWLEDGEMENTS

This work was funded by the Swiss National Science Foundation through an AMBIZIONE grant (#PZ00P2.186145) and by the MUR - Italian Minister of University and Research under the ‘‘Rita Levi-

Montalcini” program (G.M.). M.P. is supported by the European Union’s Horizon 2020 research and innovation programme under the grant agreement No. 881603 - GrapheneCore3 and the Marie Skłodowska-Curie grant agreement No. 873028, by the University of Pisa under the “PRA - Progetti di Ricerca di Ateneo” (Institutional Research Grants) - Project No. PRA_2020-2021_92

“Quantum Computing, Technologies and Applications”, and by the MUR - Italian Minister of University and Research under the “Research projects of relevant national interest - PRIN 2020” - Project No. 2020JLZ52N, title “Light-matter interactions and the collective behavior of quantum 2D materials (q-LIMA)”.

It is a great pleasure to thank Antoine Georges, Andrew Millis, and Aharon Kapitulnik for inspiring discussions.

-
- [1] P. W. Anderson, *Basic Notions of Condensed Matter Physics*, (1st edition) CRC press (1994)
- [2] See, for example, D. Jérôme, T. M. Rice, and W. Kohn, *Phys. Rev.* **158**, 462 (1967); B. I. Halperin and T. M. Rice, *Solid State Phys.* **21**, 115 (1968); B. I. Halperin and T. M. Rice, *Rev. Mod. Phys.* **40**, 755 (1968).
- [3] J. P. Eisenstein and A. H. MacDonald, *Nature* **432**, 691 (2004).
- [4] J. P. Eisenstein, *Annu. Rev. Condens. Matter Phys.* **5**, 159 (2014).
- [5] J.-J. Su and A. H. MacDonald, *Nat. Phys.* **4**, 799 (2008).
- [6] X. Liu, K. Watanabe, T. Taniguchi, B. I. Halperin, and P. Kim, *Nat. Phys.* **13**, 746 (2017).
- [7] J. I. A. Li, T. Taniguchi, K. Watanabe, J. Hone, and C. R. Dean, *Nat. Phys.* **13**, 751 (2017).
- [8] G. W. Burg, N. Prasad, K. Kim, T. Taniguchi, K. Watanabe, A. H. MacDonald, L. F. Register, and E. Tutuc, *Phys. Rev. Lett.* **120**, 177702 (2018).
- [9] A. Kogar, M. S. Rak, S. Vig, A. A. Husain, F. Flicker, Y. Il Joe, L. Venema, G. J. MacDougall, T. C. Chiang, E. Fradkin, J. van Wezel, and P. Abbamonte, *Science* **358**, 1314 (2017).
- [10] H. Cercellier, C. Monney, F. Clerc, C. Battaglia, L. Despont, M. G. Garnier, H. Beck, P. Aebi, L. Patthey, H. Berger, and L. Forró, *Phys. Rev. Lett.* **99**, 146403 (2007).
- [11] Y. F. Lu, H. Kono, T. I. Larkin, A. W. Rost, T. Takayama, A. V. Boris, B. Keimer, and H. Takagi, *Nat. Commun.* **8**, 14408 (2017).
- [12] S. S. Ataei, D. Varsano, E. Molinari, and M. Rontani, *Proc. Natl. Acad. Sci. (USA)* **118**, e2010110118 (2021).
- [13] B. Sun, W. Zhao, T. Palomaki, Z. Fei, E. Runburg, P. Malinowski, X. Huang, J. Cenker, Y.-T. Cui, J.-H. Chu, X. Xu, S. S. Ataei, D. Varsano, M. Palummo, E. Molinari, M. Rontani, and D. H. Cobden, *Nat. Phys.* **18**, 94 (2022).
- [14] D. Varsano, M. Palummo, E. Molinari, and M. Rontani, *Nat. Nanotech.* **15**, 367 (2020).
- [15] G. Mazza, M. Rösner, L. Windgätter, S. Latini, H. Hübener, A. J. Millis, A. Rubio, and A. Georges, *Phys. Rev. Lett.* **124**, 197601 (2020).
- [16] T. Kaneko, T. Toriyama, T. Konishi, and Y. Ohta, *Phys. Rev. B* **87**, 035121 (2013).
- [17] M. D. Watson, I. Marković, E. A. Morales, P. Le Fèvre, M. Merz, A. A. Haghighirad, and P. D. C. King, *Phys. Rev. Research* **2**, 013236 (2020).
- [18] L. Windgätter, M. Rösner, G. Mazza, H. Hübener, A. Georges, A. J. Millis, S. Latini, and A. Rubio, *npj Comput. Mater.* **7**, 210 (2021).
- [19] A. Subedi, *Phys. Rev. Materials* **6**, 014602 (2022).
- [20] K. Kim, H. Kim, J. Kim, C. Kwon, J. S. Kim, and B. J. Kim, *Nat. Commun.* **12**, 2998 (2021).
- [21] M. Ye, P. A. Volkov, H. Lohani, I. Feldman, M. Kim, A. Kanigel, and G. Blumberg, *Phys. Rev. B* **104**, 045102 (2021).
- [22] D. Golež, S. K. Y. Dufresne, M.-J. Kim, F. Boschini, H. Chu, Y. Murakami, G. Levy, A. K. Mills, S. Zhdanovich, M. Isobe, H. Takagi, S. Kaiser, P. Werner, D. J. Jones, A. Georges, A. Damascelli, and A. J. Millis, *Phys. Rev. B* **106**, L121106 (2022).
- [23] K. Katsumi, A. Alekhin, S.-M. Souliou, M. Merz, A.-A. Haghighirad, M. Le Tacon, S. Houver, M. Cazayous, A. Sacuto, and Y. Gallais, *arXiv:2211.08537*.
- [24] M. Michael, S. R. Ul Haque, L. Windgätter, S. Latini, Y. Zhang, A. Rubio, R. D. Averitt, and E. Demler, *arXiv:2207.08851*.
- [25] B. A. Volkov and Yu. V. KopaeV, *JETP* **27**, 7 (1978).
- [26] B. A. Volkov, V. L. Ginzburg, and Yu. V. KopaeV, *JETP* **27**, 206 (1978).
- [27] A. Amaricci, G. Mazza, M. Capone, and M. Fabrizio, *Phys. Rev. B* **107**, 115117 (2023).
- [28] N. Marzari, A. A. Mostofi, J. R. Yates, I. Souza, and D. Vanderbilt, *Rev. Mod. Phys.* **84**, 1419 (2012).
- [29] D. Bohm, *Phys. Rev.* **75**, 502 (1949).
- [30] See the Supplemental Material file, which contains details on the model and the variational wave-function optimization and the comparison between the cylinder and infinite sheet geometry. Supplemental materials contains citations to Refs. [31–34]
- [31] J. Li, D. Golez, G. Mazza, Andrew J. Millis, A. Georges, and M. Eckstein, *Phys. Rev. B* **101**, 205140 (2020).
- [32] O. Di Stefano, A. Settineri, V. Macrì, L. Garziano, R. Stassi, S. Savasta, and F. Nori, *Nat. Phys.* **15**, 8 (2019).
- [33] I. Amelio, L. Korosec, I. Carusotto, and G. Mazza, *Phys. Rev. B* **104**, 235120 (2021).
- [34] O. Dmytruk and M. Schiró, *Phys. Rev. B* **103**, 075131 (2021).
- [35] G. Mazza and A. Georges, *Phys. Rev. Lett.* **122**, 017401 (2019).
- [36] G. M. Andolina, F. M. D. Pellegrino, V. Giovannetti, A. H. MacDonald, and M. Polini, *Phys. Rev. B* **100**, 121109 (2019).
- [37] P. Nataf, T. Champel, G. Blatter, and D. M. Basko, *Phys. Rev. Lett.* **123**, 207402 (2019).
- [38] G. M. Andolina, F. M. D. Pellegrino, V. Giovannetti, A. H. MacDonald, and M. Polini, *Phys. Rev. B* **102**, 125137 (2020).
- [39] D. Guerci, P. Simon, and C. Mora, *Phys. Rev. Lett.* **125**, 257604 (2020).
- [40] G. M. Andolina, F. M. D. Pellegrino, A. Mercurio, O. Di Stefano, M. Polini, and S. Savasta, *Eur. Phys. J. Plus* **137**, 1348 (2022).
- [41] H. Hübener, U. De Giovannini, C. Schäfer, J. Andberger,

- M. Ruggenthaler, J. Faist, and A. Rubio, *Nat. Mater.* **20**, 438 (2021).
- [42] C. Guo, C. Putzke, S. Konyzheva, X. Huang, M. Gutierrez-Amigo, I. Errea, D. Chen, M. G. Vergniory, C. Felser, M. H. Fischer, T. Neupert and P. J. W. Moll *Nature* **611**, 461 (2022)
- [43] F. Grandi, A. Consiglio, M. A. Sentef, R. Thomale and D. M. Kennes *Phys. Rev. B* **107**, 155131 (2023)
- [44] M. Serlin, C. L. Tschirhart, H. Polshyn, Y. Zhang, J. Zhu, K. Watanabe, T. Taniguchi, L. Balents, and A. F. Young, *Science* **367**, 900 (2019).
- [45] C. L. Tschirhart, M. Serlin, H. Polshyn, A. Shragai, Z. Xia, J. Zhu, Y. Zhang, K. Watanabe, T. Taniguchi, M. E. Huber, and A. F. Young, *Science* **372**, 1323 (2021).
- [46] K. P. Nuckolls, M. Oh, D. Wong, B. Lian, K. Watanabe, T. Taniguchi, B. A. Bernevig, and A. Yazdani, *Nature* **588**, 610 (2020).
- [47] P. Stepanov, M. Xie, T. Taniguchi, K. Watanabe, X. Lu, A. H. MacDonald, B. A. Bernevig, and D. K. Efetov, *Phys. Rev. Lett.* **127**, 197701 (2021).
- [48] Y. Xie, A. T. Pierce, J. M. Park, D. E. Parker, E. Khalaf, P. Ledwith, Y. Cao, S. H. Lee, S. Chen, P. R. Forrester, K. Watanabe, T. Taniguchi, A. Vishwanath, P. Jarillo-Herrero, and A. Yacoby, *Nature* **600**, 439 (2021).
- [49] G. Chen, A. L. Sharpe, E. J. Fox, Y.-H. Zhang, S. Wang, L. Jiang, B. Lyu, H. Li, K. Watanabe, T. Taniguchi, Z. Shi, T. Senthil, D. Goldhaber-Gordon, Y. Zhang, and F. Wang, *Nature* **579**, 56 (2020).
- [50] J. Xia, Y. Maeno, P. T. Beyersdorf, M. M. Fejer, and A. Kapitulnik, *Phys. Rev. Lett.* **97**, 167002 (2006).
- [51] G. E. Volovik, *The Universe in a Helium Droplet* (Oxford University Press, Oxford, 2003).
- [52] B. A. Bernevig and T. L. Hughes, *Topological Insulators and Superconductors* (Princeton University Press, Princeton, 2013)
- [53] X.-L. Qi and S.-C. Zhang, *Rev. Mod. Phys.* **83**, 1057 (2011).
- [54] C. Kallin and J. Berlinsky, *Rep. Prog. Phys.* **79**, 054502 (2016).